of this approach in which cyclics containing equal numbers of dimethyl- and methylsiloxy groups were condensed with 3-vinyl-7-oxabicyclo[4.1.0]heptane and other epoxides. Table III also records the cure and T_g data obtained from the UV cure of these same monomers. Especially notable in this table are the high values obtained for those monomers containing cycloaliphatic epoxide groups after only 5 s of irradiation. In a similar manner, monomers having variable degrees of epoxide functionality can be prepared by using cyclic substrates derived by cracking the appropriate poly(dimethylsiloxane-*co*-methylsiloxane) copolymer and then carrying out the platinum-catalyzed hydrosilylation with a vinyl-substituted epoxide. As with the other cyclic epoxysilicone monomers prepared and described in Table I, the monomers reported above have excellent chemical resistance (very high gel contents) and hardness (pencil hardness *H* and above), which make them attractive for coatings applications.

Conclusions

In this paper we have described the development of a new method for the preparation of cyclic poly(siloxanes) from linear poly(siloxanes) by a nonequilibrium thermal depolymerization process. Zeolite fixed bed catalysts are preferred for this process, giving high yields of uncontaminated cyclic products. In addition, they are commercially available, inexpensive materials that are highly active, easy to use, and may be recycled without loss of activity. The depolymerization is carried out at temperatures from 400 to 800 °C, under which conditions the cyclic products flash away from the reaction zone, eliminating potential explosion and fire hazards. Last, the products of thermal cracking are eminently useful. Of particular interest are the cyclic epoxysilicone monomers which can be prepared directly from the cracking distillate. These monomers together with onium salt photoinitiators are exceptionally reactive substrates for UV curing applications because of their high rates of cure and excellent mechanical and chemical properties. Such rapidly curing systems are particularly useful for UV cured coatings, printing inks, and electronic encapsulations.

Acknowledgment. We acknowledge the generous gift of an analytical sample of mixed Si-H cyclics from D. Gross of the General Electric Silicone Products Business Division. We also thank W. Ligon and R. May for running the GC-MS characterization of the cyclic poly(siloxanes).

Electronic Structure of a New Ternary Chalcogenide: $NbNiTe_5$

Jean-François Halet† and Roald Hoffmann*

Department of Chemistry and Materials Science Center, Cornell University, Ithaca New York 14853

Wolfgang Tremel

Anorganisch-Chemisches Institut, Universität Münster, Wilhelm-Klemm-Strasse 8, D-4400 Münster, FRG

Eric W. Liimatta and James A. Ibers

Department of Chemistry, Northwestern University, Evanston, Illinois 60208

Received January 30, 1989

An attempt at analyzing the electronic structure and bonding in the metallic and paramagnetic compound $NbNiTe_5$ has been made, using extended Hückel tight-binding calculations. The metallic behavior of this compound originates primarily from Te 5p states. Rather anisotropic conductivity is expected. It is difficult to assign a definitive oxidation state to the elements in this compound, but we suggest that an oxidation formalism of $(Nb^{3+})(Ni^{2+})(Te)_5^{5-}$ may be appropriate. This accounts for the numerous Te-Te contacts and electronegativity considerations but not for the magnetic measurements. The bonding between tellurium and transition-metal atoms is highly covalent; the compound can be considered as an intermetallic phase. The title compound and its Ta and Pd derivatives are compared, as well as some layerlike rare-earth-metal tellurides.

The Structure

The interesting properties, metallic *and* paramagnetic, displayed by the recently characterized compound $NbNiTe_5$[1] prompted us to study its electronic structure. The D_{2h}^{17}-*Cmcm* structure of $NbNiTe_5$ forms a new layered structural type. Each layer is made of infinite chains of face-sharing bicapped trigonal $NbTe_8$ prisms running through the structure parallel to the *a* axis. The one-dimensional chains are brought together in an up and down fashion along the *c* axis, as for $ZrTe_5$.[2] But this time the structure is assembled so that the Te atoms of two adjacent chains form chains of octahedra where the Ni atoms are trapped. In other words, the one-dimensional chains of bicapped trigonal prisms (BCTP) are linked together via "intercalated" octahedral nickel atoms. This is depicted in Figure 1.

No close metal-metal contacts are observed in the crystal. The shortest Nb···Nb and Ni···Ni distances are

†Permanent address: Laboratoire de Cristallochimie, UA 254, Université de Rennes I, 35042 Rennes, France.

(1) Liimatta, E. W.; Ibers, J. A. *J. Solid State Chem.* **1987**, *71*, 384.
(2) Furuseth, S.; Brattas, L.; Kjekshus, A. *Acta Chem. Scand.* **1973**, *27*, 2367.

0897-4756/89/2801-0451$01.50/0

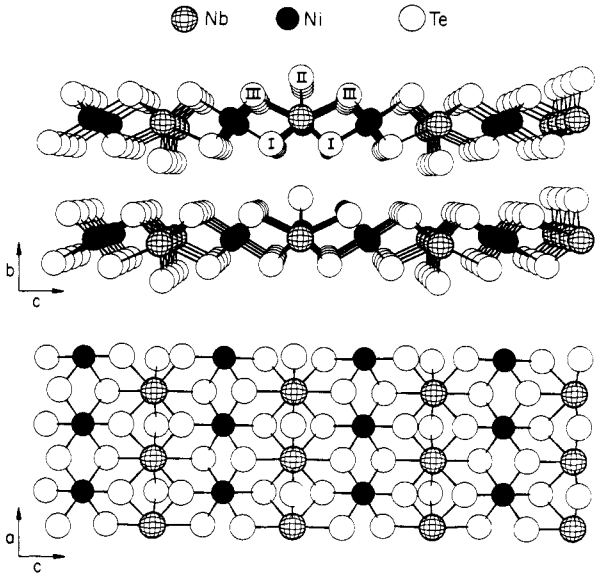

Figure 1. (100) and (010) projections of the $NbNiTe_5$ structure.[1] Filled circles are Ni atoms, hatched circles are Nb atoms, and open circles are Te atoms.

3.656 Å and the Nb···Ni separation is 4.2 Å. The shortest Te–Te contacts are 3.196 and 3.331 Å. This is only ca. 10% and 14%, respectively, longer than the usual distance of 2.92 Å expected for a Te–Te single bond.[3] Therefore, weak Te–Te interactions must be present in $NbNiTe_5$. If BCTP Nb^{5+} (d^0) and octahedral Ni^{4+} (d^6) metal atoms are assumed, then the oxidation formalism (and this is only a formalism) leads to $(Nb^{5+})(Ni^{4+})(Te)_5^{9-}$. Since the compound exhibits metallic behavior ($\sigma_{295} \sim 1.3 \times 10^4\ \Omega^{-1}\ cm^{-1}$), one might think that the unsaturated Te band is responsible for the conduction properties of the material. In addition, some electron transfer from the Te bands to Nb or Ni to account for the measured μ_{eff} of 1.24 μ_B has been suggested.[1] We will return to a discussion of the oxidation states in this structure.

It is always useful to look at structures in alternative ways. There is another way to assemble (mentally) the $NbNiTe_5$ structure, namely, from $NbTe_3$ trigonal prism blocks and edge-sharing square-planar $NiTe_2$ chains. The end-face sharing prism motifs are familiar from the structures of early transition-metal chalcogenides such as $ZrTe_3$, 1,[4] $ZrTe_5$,[2] and other related compounds. The edge-sharing chains, **2**, are well-known from the structures of platinum-group metal sulfides such as PtS[5] and K_2PtS_2.[6] In the view of **1**, the $ZrTe_3$ structure, we are looking down the shared triangular faces of the Te trigonal prisms. The prisms are so arranged that the Zr atoms acquire two additional Te contacts from neighboring chains, the interprism Zr–Te distances being only slightly longer than the intraprism ones. As a result the Zr atoms reside in a bicapped trigonal prismatic environment. A similar Zr coordination is found in $ZrTe_5$. Here a Te_2 group takes the position of the apical Te atom. Interestingly, with the exception of $NbNiTe_5$, no analogous Nb–Te compounds have been made so far.

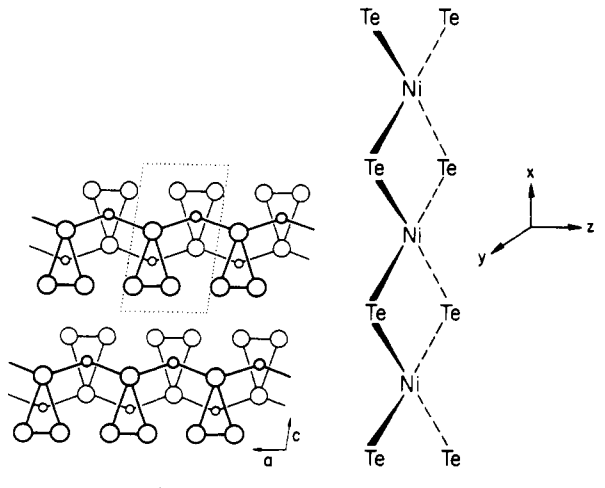

1 2

In $NbNiTe_5$ two $NiTe_2$ fragments complete the coordination of the central Nb atom. In addition, the Te_I atoms of the basal Te_2 group approach the Ni atoms from above and below the plane to give an almost perfect octahedral Ni coordination. In other words, we see coordination chemistry in the solid state.[7] $NbTe_3$ and $NiTe_2$ fragments are mutually coordinated to each other to give a three-dimensional structure. The trigonal prism blocks and square planar chains are clearly visible in the lower part of Figure 1.

Building Up the Electronic Structure of $NiNiTe_5$

It is instructive to pursue a dual development of the orbitals of $NbNiTe_5$. So let us return to the local environment around the Nb atom in the composite structure. It is approximately bicapped trigonal prismatic. Presumably the Nb block splits into a one-below-four pattern above the ligand Te p orbital set. There are no substantial Nb–Nb or Te–Te interactions along or between chains in the solid compound. Therefore this schematic orbital pattern is almost sufficient for a crude description of the appearance of the density of states (DOS) of the solid. We just need to take into consideration the perturbation introduced by the Ni atoms encapsulated in the octahedral holes. The d block of the octahedral Ni atoms will split into t_{2g} and e_g combinations, interacting with some Te p levels. Because nickel is between niobium and tellurium in the electronegativity scale of the elements,[8] we expect the empty e_g set to be positioned beneath the Nb d orbitals and the occupied t_{2g} set to be buried in the top of the Te p band. Thus a density of states such as **3** is expected. This corresponds formally to a $Ni^{4+}(d^6)$, $Nb^{5+}(d^0)$ configuration, leaving Te_5 formally as 9–. The Te_5 5 p band has room for 30 electrons, which would correspond to Te_5^{10-}. The Te levels are thus not completely filled by electrons, so the Fermi level would lie somewhat beneath the top of the Te 5 p band, accounting for the metallic behavior of the compound.

These expectations are based on a crystal field model which first fills the anion valence shells and then considers the remaining cation electrons to determine the properties of a material. In fact, such an ionic picture is often oversimplified for tellurides. The large size of the Te atoms induces important overlaps between their p orbitals and thus broadens the corresponding bands even at fairly large separations. Many molecular and solid compounds exhibit Te···Te contacts in the range 3.00–3.30 Å, i.e., ca. 5–15% longer than a Te–Te single bond. Significant Te–Te

(3) Brostigan, G.; Kjekshus, A. *Acta Chem. Scand.* **1970**, *24*, 1925.
(4) (a) Brattas, L.; Kjekshus, A. *Acta Chem. Scand.* **1972**, *26*, 3441. (b) Furuseth, S.; Brattas, L.; Kjekshus, A. *Acta Chem. Scand.* **1975**, *A29*, 623.
(5) Krebs, H. *Grundzüge der anorganischen Kristallchemie*; Ferdinand Enke Verlag: Stuttgart, 1968.
(6) Bronger, W. *Angew. Chem.* **1981**, *93*, 12; *Angew. Chem., Int. Ed. Engl.* **1981**, *20*, 52.
(7) Sunshine, S. A.; Keszler, D. A.; Ibers, J. A. *Acc. Chem. Res.* **1987**, *20*, 395.
(8) Pauling, L. *The Nature of the Chemical Bond*; Cornell University Press: Ithaca, NY, 1960; p 93.

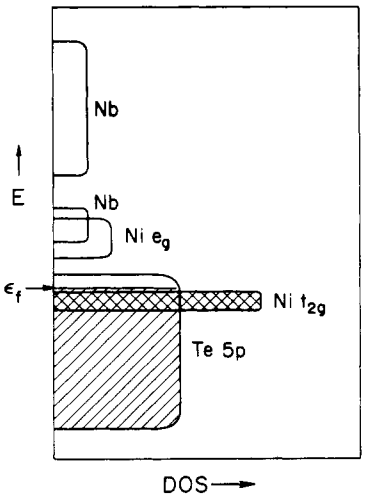

bonding interactions have been noticed at contacts as large as 3.50 Å. For instance, the Te 5p band in the layered $NiTe_2$ compound, where the Ni atoms are in an octahedral environment, spreads over a 10-eV range, even though the shortest Te–Te separations are of the order of 3.40 Å.[9] Moreover, the electronegativity difference between tellurium and transition-metal atoms is relatively small (for example, 0.2 and 0.5 for Ni and Nb, respectively).[8] These two criteria, large atomic size and small electronegativity difference, explain why the bonding in tellurides is mainly covalent rather than ionic.

A highly distorted metal-centered bicapped trigonal prismatic geometry is a common feature of binary and ternary chalcogenides of the group IV and V triads, which adopt this type of coordination.[2,10] $NbNiTe_5$ is not an exception. Nevertheless, the distortion observed in the title compound is less important than in the other BCTP chalcogenides. In **4** some particular atom–atom separations in $NbNiTe_5$ are compared to those observed in $HfTe_5$, which is a typical example of a BCTP metal chalcogenide. In both cases the Te atoms of the prisms form isosceles triangles, and two sides of each triangle are rather longer than the remaining side. In compounds such as $HfTe_5$, two Te ligands are really transformed into a coordinated Te_2 entity. Consequently a vacant antibonding orbital deriving from Te 5p orbitals is pushed above the metal d orbitals.[11] The distortion observed in $NbNiTe_5$ is less drastic, since no strong Te–Te pairings are encountered (see **4**). The distance ratio $d(Te_I–Te_I)/d(Te_I–Te_{II})$ is 0.81, while it is only 0.67 in the $HfTe_5$ case. Note that Te–Te intertriangle separations in the two compounds do not differ much (3.656 and 3.974 Å in $NbNiTe_5$ and $HfTe_5$, respectively). The molecular orbital pattern of a hypothetical irregular BCTP $NbTe_8^{11-}$ complex, modeled in C_{2v} symmetry after the solid structure, is illustrated on the left-hand side of Figure 2. A weak perturbation of the electronic structure of the regular BCTP is observed upon distortion. The Nb 4d orbitals split to give a one-below-four orbital pattern. The slightly antibonding Nb–Te $1a_1$ orbital, mainly a mixture of $x^2 - y^2$ and z^2, is substantially separated from the four other d levels. Because of the diffuseness of the Te 5p orbitals, the top of the ligand Te 5p "band" lies at rather high energy. Two levels, mainly $Te_I–Te_I$ and $Te_I–Te_{III}$ antibonding, are positioned just above the $1a_1$ Nb d level, which is therefore occupied for the given electron count of $NbTe_8^{11-}$. The distortion from an idealized C_{2v} structure has been discussed previously in detail,[12] as a function of the metal d electron count (i.e., d^0 with $1a_1$ vacant vs d^2 with $1a_1$ occupied).

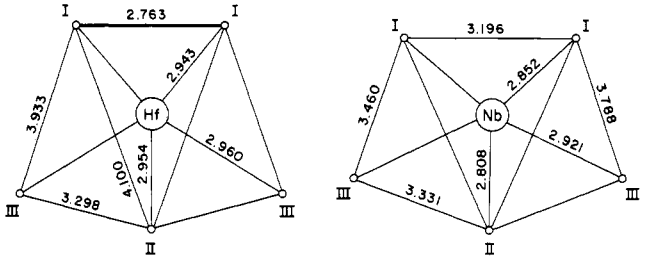

4

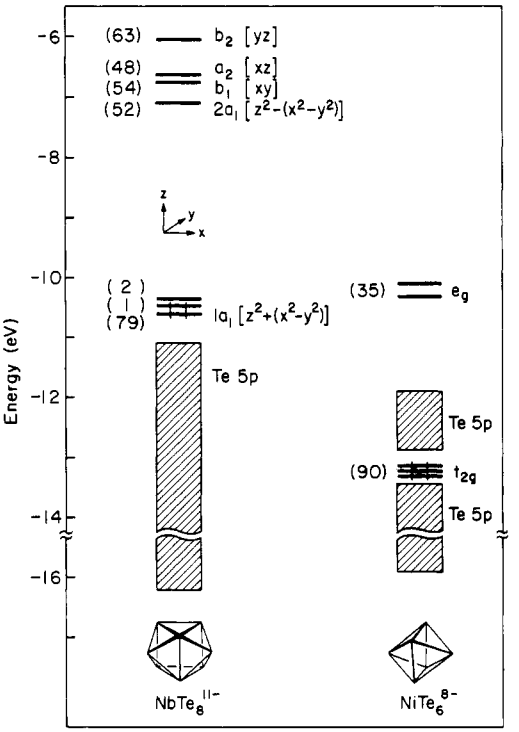

Figure 2. Molecular orbitals of BCTP $NbTe_8^{11-}$ and octahedral $NiTe_6^{8-}$ monomers. The numbers in parentheses indicate the percentage metal character.

The environment around the Ni atoms is almost octahedral. Molecular orbital calculations performed on a $NiTe_6^{8-}$ complex show that Te–Te 5p antibonding levels are intercalated between the Ni e_g and t_{2g} blocks, again because of the diffuseness of the Te atomic orbitals (see the right-hand side of Figure 2). Note that the Ni e_g levels are in resonance with the $1a_1$ orbital and the top of the Te 5p "band" of the $NbTe_8^{11-}$ monomer. The numbers in parentheses in Figure 2, indicating the percentage metal character, show the substantial participation of the Te orbitals in the Nb and Ni "d levels". This anticipates highly covalent bonding in $NbNiTe_5$.

Considering the alternative construction of $NbNiTe_5$ from $NbTe_3$ and $NiTe_2$ fragment chains, there is another way to rationalize its electronic structure in a straightforward manner. The energy levels of a $NbTe_6^{7-}$ trigonal prism, in the C_{2v} local symmetry of the title compound, are shown in **5**. The d-block splitting is close to the familiar one and two (z^2; $x^2 - y^2$, xy) below two (xz, yz) for

(9) Guo, G. Y.; Liang, W. Y. *J. Phys. C: Solid State Phys.* **1986**, *19*, 5365.

(10) See for example: (a) Bjerkelund, E.; Kjekshus, A. *Acta Chem. Scand.* **1965**, *19*, 701. (b) Sunshine, S. A.; Ibers, J. A. *Inorg. Chem.* **1986**, *25*, 4355.

(11) (a) Bullett, D. W. *Solid State Commun.* **1982**, *42*, 691.

(12) Burdett, J. K.; Hoffmann, R.; Fay, R. C. *Inorg. Chem.* **1978**, *17*, 2553.

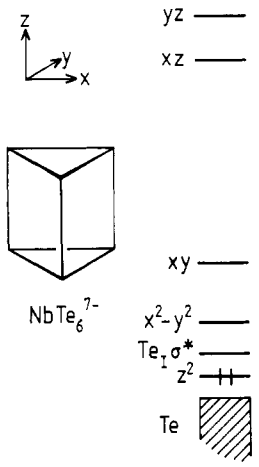

5

trigonal prismatic coordination.[13] The Te_I–Te_I σ^* is found vacant, but at a rather low energy, between the Nb z^2 and $x^2 - y^2$ orbitals. This is due to the relatively long Te_I–Te_I distance (3.19 Å). For Nb^{5+} the d block is empty. We note two low-lying acceptor orbitals ($x^2 - y^2$, xy) pointing to the rectangular faces of the prism. When the central Nb atom acquires two additional capping ligands in its coordination sphere, these orbitals will be perturbed substantially and they will be pushed up by the ligand field. The result is a one-below-four orbital pattern in the metal d block, the typical electronic feature of eight-coordination. We have seen this in Figure 2.

We can model the square-planar chain by a $NiTe_4$ unit, the orbitals of which are shown in **6**. There is a natural gap between four lower lying d orbitals and the xy; this

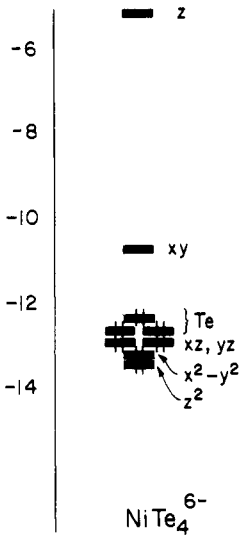

6

is typical of square-planar coordination. This leads us to a tentative assignment of a d^8, Ni^{2+} configuration as being a natural one for this unit. That in turn puts a $NiTe_4^{6-}$ charge on the monomer model. In addition we notice a potential acceptor orbital, mainly Ni z, pointing away from Ni and waiting for electron density from an approaching atom.

When the $NbTe_6^{7-}$ and $NiTe_4^{6-}$ monomers are condensed to infinite chains, the monomer levels spread out into bands, the band width depending on the orbital overlap. Some bands may acquire quite substantial dispersion. The acceptor orbitals, however, do not interact much, for they stick out into innocent regions of space. Therefore the corresponding states are well-localized in relatively narrow bands.

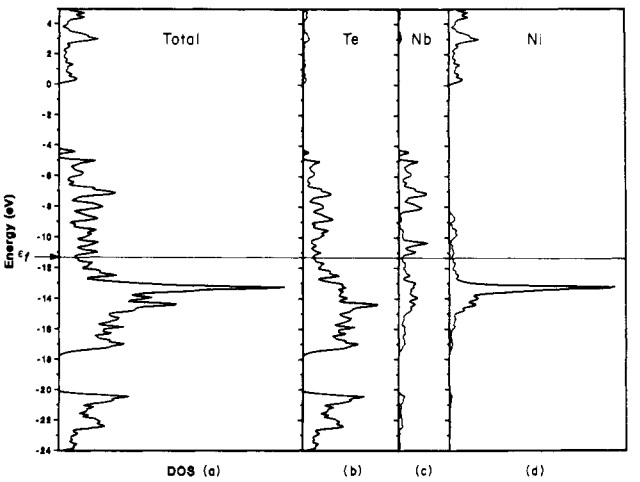

Figure 3. DOS of 2-D $NbNiTe_5$: (a) total DOS; (b) contribution of Te atoms; (c) contribution of Nb atoms; (d) contribution of Ni atoms.

Now we interact $NbTe_3$ prism stacks and $NiTe_2$ chains. There is a typical donor–acceptor interaction, the donor states being Te lone pairs of the $NbTe_3$ and $NiTe_2$ fragments, the acceptor states having substantial Nb $x^2 - y^2$, xy, and Ni z character, respectively. The interactions are relatively easy to trace back. The remnant of the Ni p band is pushed up in energy. The Nb $x^2 - y^2$, xy states are affected in a similar fashion. Initially located in a narrow interval at the bottom of the d block, they are pushed up and spread out into a relatively broad band. Charge is transferred from the Te to the Ni and Nb atoms. One could assume that low-lying Ni states are filled at the expense of higher lying Te ones. On the other hand there will be some "back donation" from filled Ni d orbitals, mainly z^2, into empty Te–Te antibonding orbitals. This "back donation" weakens the Te–Te bond in the prism and manifests itself in a slight increase of the Te–Te distances from 2.9 Å (in $ZrTe_3$) to 3.2 Å (in $NbNiTe_5$). These simple considerations show that the structure of $NbNiTe_5$ is strongly stabilized by donor–acceptor interactions. So it is for related early-transition-metal chalcogenides, which contain fused MX_3 prism blocks.

We are ready now to attempt to unravel the bonding properties of $NbNiTe_5$, by carrying out tight-binding calculations[14] using the extended Hückel formalism.[15] The computational details are gathered in the Appendix. The layers in the title compound are held together through van der Waals forces, so calculations were first performed on a two-dimensional material.

Conductor...

The DOS extracted from a calculation on a two-dimensional $NbNiTe_5$ layer separates broadly into three parts (see Figure 3). The lowest part, centered at −21 eV, derives predominantly from the Te 5s orbitals. Its splitting into two subbands suggests some Te–Te interaction (mainly Te_I–Te_I). The bands that form the middle region, extending over the energy range −4 to −18 eV, are made up mainly from the metal d orbitals (Nb 4d and Ni 3d)

(13) Hoffmann, R.; Shaik, S.; Scott, J. C.; Whangbo, M.-H.; Foshee, M. J. *J. Solid State Chem.*, **1980**, *34*, 263.

(14) (a) Whangbo, M.-H.; Hoffmann, R. *J. Am. Chem. Soc.* **1978**, *100*, 6093. (b) Whangbo, M.-H.; Hoffmann, R.; Woodward, R. B. *Proc. R. Soc. London, Ser. A* **1979**, *366*, 23.

(15) Hoffmann, R. *J. Chem. Phys.* **1963**, *39*, 1397.

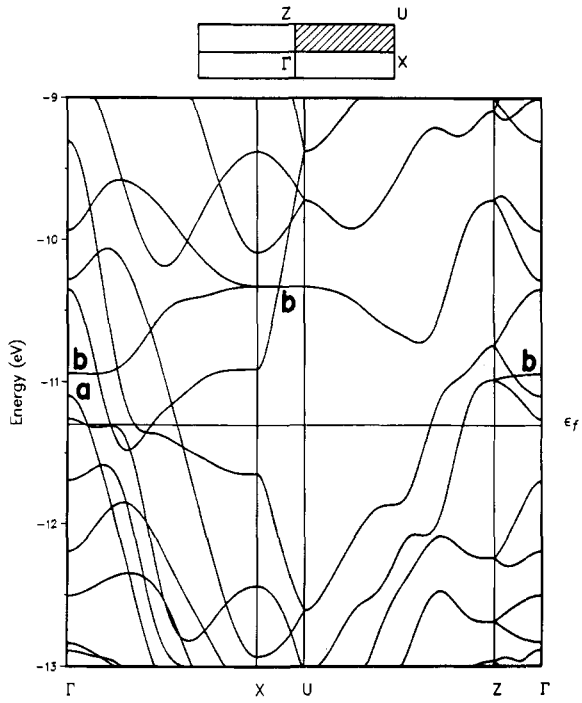

Figure 4. Band structure of two-dimensional $NbNiTe_5$.

and the Te 5p orbitals. Decomposition of the contributions to this DOS of the different elements is illustrated on the right-hand side of Figure 3. The overall band width of the metal d/tellurium p manifold, about 14 eV, is essentially due to the bonding–antibonding gap between Te 5p orbitals (see Figure 3b). The Nb 4d band spreads over 13 eV while the Ni 3 d band spans over 8 eV. Note the sharp peaked t_{2g} band of the Ni atoms in Figure 3d. Its position around −13.5 eV, which corresponds to the ionization potential of the Ni 3d atomic orbitals, indicates the rather nonbonding character of these states. Finally, the Nb and Ni p states lie higher in energy by several electronvolts.

As we can see in Figure 3, the metal d and tellurium p bands are rather wide and overlap considerably. This points to strong covalent character in the bonding of this material, as shown by the tellurium–metal overlap populations (Te–Ni, 0.31; Te–Nb, 0.38/0.48). The Te–Te interactions, explicit in Figure 3, manifest themselves through the Te–Te overlap populations, which while small are definitely positive (Te_I–Te_I, 0.09; Te_I–Te_{III}, 0.01; Te_{II}–Te_{III}, 0.08). We think there might be a weak Nb–Nb interaction along the BCTP chains. The computed Nb–Nb overlap population is nearly zero but positive: 0.02. According to the calculations, a little electron density is transferred from the Te atoms toward the Nb and Ni atoms. The calculated atomic net charges are the following:

$$(Nb^{0.55-})(Ni^{0.22-})(Te_I^{0.14+})_2(Te_{II}^{0.18+})(Te_{III}^{0.13+})_2$$

The position of the Fermi level at −11.3 eV, in a rather deep but nonzero minimum in the density of states, predicts quite clearly that $NbNiTe_5$ should be metallic. This might occur through Te 5p carriers since the DOS for both Nb and Ni atoms is very small (see Figure 3c,d). The metallic behavior is confirmed in Figure 4, where some calculated electron bands of $NbNiTe_5$ are illustrated along high symmetry lines. Because of a screw axis along the *a* axis and a glide plane (perpendicular to *b*) present in $NbNiTe_5$ layers, all bands are doubly degenerate along the symmetry line *UZ*.

The bands around the Fermi level are rather dispersive, particularly along the lines $\Gamma \rightarrow X$ and $U \rightarrow Z$, parallel to the a^* axis. The Fermi level cuts through several bands along these lines but not along the symmetry lines $X \rightarrow U$ and $Z \rightarrow \Gamma$, parallel to the c^* axis. High conductivity is expected along *a*, in agreement with experiment.[1]

To gain some insight into how the band structure of $NbNiTe_5$ is related to its physical properties, we have to take a closer look at some of the bands close to the Fermi level. In fact, several of them can be identified as a combination of $NbTe_3$ and $NiTe_2$ fragment bands. For instance, **7**, marked **a** in Figure 4, clearly is a combination

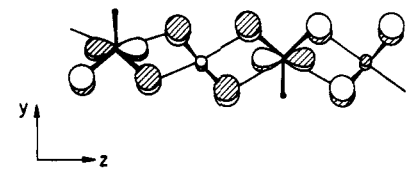

7

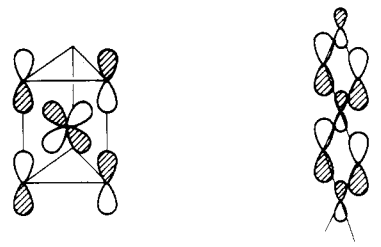

8 **9**

of **8** and **9**, and its nodal properties force it to lower energies as we move along Γ–X. Note the band marked **b**, which exhibits only a small dispersion along Γ–X and continues virtually flat along the line X–U. Similarly, this band is flat along Γ–Y. An explanation can easily be given from the band composition. The corresponding crystal orbital has been drawn out in **10** with its topology at the

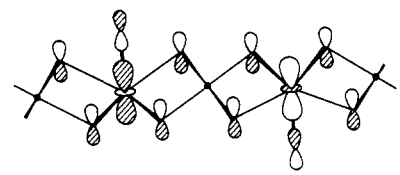

10

zone center Γ. The band has substantial Nb y^2 character with some small amounts of Te *y* contributions along all the symmetry lines shown. As a result there are weak π interactions between the tellurium and mostly δ interactions between the niobium atoms. No wonder that this band is dispersionless.

The carrier states at the Fermi level originate primarily from Te atoms. At the zone center Γ, the bands crossed by the Fermi level consist mainly of Te 5p orbitals oriented along the *a* axis. The Te–Te antibonding bands, which mix with other lower bands of the same symmetry along the line $\Gamma \rightarrow X$, possess some Ni or Nb contribution. According to Figure 4, hole pockets are found at Γ and electron pockets along the symmetry line $\Gamma \rightarrow X$.

We must discuss the assignment of the oxidation states to the elements in this fascinating structure. It is clear that oxidation states are a formalism, albeit a tremendously useful one. Real charges on atoms in any structure, be it molecular or ionic, are unlikely to be outside the range +1 to −1, as Pauling pointed out some time ago. The calculations cited earlier in this section do not show great departure from electroneutrality, yet a formalism consistent with that, $(Nb^0)(Ni^0)(Te)_5^0$ is not very informative. We think that one must accept the ambiguity of any charge distribution but still take account of local crystal field splittings, geometries, and experimental measurements and

try to assign formal oxidation states.

In the case at hand, the geometries around Ni and Nb push one toward a $(Nb^{5+})(Ni^{4+})(Te)_5^{9-}$ assignment. This is clearly an extreme of charge transfer. Figure 2 (model clusters for the extended structure) shows that the Nb d levels and the Ni e_g band are within 1 eV of the top of the Te 5p band. There is clearly much mixing and substantial electron transfer. We think that a formalism such as $(Nb^{3+})(Ni^{2+})(Te)_5^{5-}$ may be an appropriate compromise. Holes in the Te 5p band $\{(Te)_5^{9-}$ or $(Te)_5^{5-}\}$ are consistent with the numerous Te···Te interactions seen in the structure.

...and Paramagnetic

A detailed analysis of the shape of the Fermi surfaces associated with the bands crossed by the Fermi level may not be appropriate since the compound exhibits some paramagnetism as well as conduction. We are thus uncertain as to where the Fermi level lies; that indicated in the figures is for a paired occupation, low-spin state.

One-electron band theory leads to the prediction of either a metallic or an insulating material. Electron–electron repulsion is neglected in our calculations, and consequently magnetism is not properly described. However, it is worth speculating on the origin of the magnetic properties of the title compound. We have seen previously that the covalent character in $NbNiTe_5$ was sufficiently important to consider it an intermetallic phase rather than an ionic compound. Temperature-independent Pauli paramagnetism or "itinerant" magnetism is expected in metallic compounds when electrons close to the Fermi level move around rather freely in the crystal. Their wave functions are delocalized, and therefore their associated bands are dispersive. This is to be distinguished from the temperature-dependent magnetism that arises from localized electrons associated with narrow bands and a high density of states. Magnetic susceptibility due to itinerant electrons is usually small relative to that due to localized electrons.

The measured magnetic moment μ_{eff}, 1.24 μ_B, is small and close to 1.73 μ_B, the value expected for one unpaired electron. Such a value is characteristic of Pauli paramagnetism. However the magnetic susceptibility obeys overall the Curie–Weiss law associated with localized moments, and this is not characteristic of Pauli paramagnetism. Our description of the magnetism of this compound remains incomplete.

One intriguing fact is that the computed Fermi level lies close to some flat bands. The flatness of these bands is defined sufficiently well and they are located sufficiently close to ϵ_f that the observed magnetic properties of the system may be accounted for. Moreover, since the niobium contribution to **10** is large, its location on the energy scale is almost invariant—close to −11 eV, where the Nb 4d valence-shell ionization potential puts it.

Several strongly covalent tellurides are known.[16] The Te–Te distances in these compounds are in the range between 3.0 and 3.5 Å, and these materials are best characterized as alloys. Prominent examples are the layered transition-metal ditellurides MTe_2[17] or the layerlike rare-earth polytellurides.[17] On the other hand, many compounds exist where Te can be viewed in the ionic limit as Te^{2-}. These materials are more ionic and they obey the usual electron-counting (Mooser–Pearson, Zintl) rules.[18] The remarkable point about tellurium (and the other elements along the "Zintl line", the diagonal of the periodic system) is that they are borderline cases. Tellurium compounds can be ionic materials and alloys just as well. This ambivalence also becomes apparent in the structure of molecular compounds, one nice example here being the recently synthesized $NbTe_{10}^{3-}$ anion.[19] One can blame mainly two factors for the "anomalous" behavior: (1) the diffuse Te 5p orbitals and (2) the inert electron-pair effect,[20] which is known for heavy elements to contract the 5s orbital and to lower its energy. The general result for heavy main-group elements is reduced lone-pair repulsion. The first factor was operative in $NbNiTe_5$. A typical consequence of the second factor is the increased tendency of tellurium to be hypervalent, as in the rare-earth-metal polytellurides, which are briefly discussed in the next section.

Layerlike Rare-Earth-Metal Tellurides

To calibrate the Te–Te interactions observed for intermediate Te–Te distances of 3.1–3.2 Å in $NbNiTe_5$, we have done calculations on several rare-earth-metal polytellurides, where Te–Te separations in this range have been observed as well. Two structures have been determined, $NdTe_3$[21] and Nd_2Te_5,[22] but various combinations of these two prototypes are known. All of them are based on the Fe_2As(C38) structure.[23] Schematic representations of $LnTe_2$ and $LnTe_3$ are given in **11** and **12**. The Fe_2As-like $LnTe_2$ structure is layerlike, but it exhibits three-dimensional bonding properties as well.

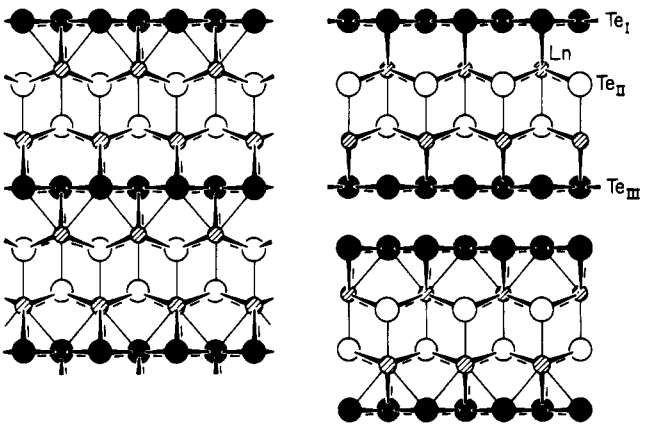

11 **12**

The $LnTe_2$ structure is built up from layers of square nets, coming out perpendicular to the plane of the paper. There are two associated square nets of Ln and Te_{II} atoms. They are separated by one layer of Te_I atoms, which is twice as dense as the Ln and Te layers. The structural units in the $LnTe_3$ structure have one additional Te layer inserted. In the unit cell of the pseudotetragonal $LnTe_3$ structure two of these $LnTe_3$ units are stacked to give a C-centered orthorhombic unit cell. The Ln_2Te_5 structure, $LnTe_2{\cdot}LnTe_3$, is made up of $LnTe_2$ and $LnTe_3$ units. In all three structure types the Ln atoms are in a nine-coordinate environment. The Te_I–Te_I contacts in the basal plane of all three structures at 3.18 Å are significantly

(16) Böttcher, P. *Angew. Chem.* **1988**, *100*, 781; *Angew. Chem., Int. Ed. Engl.* **1988**, *27*, 759.
(17) Hulliger, F. *Structural Chemistry of Layer-Type Phases*; Levy, F., Ed.; Reidel: Dordrecht, The Netherlands, 1976.
(18) Pearson, W. B. *The Crystal Chemistry and Physics of Metals and Alloys*; Wiley-InterScience: New York, 1972.
(19) Flomer, W. A.; Kolis, J. W. *J. Am. Chem. Soc.* **1988**, *109*, 3682.
(20) (a) Pitzer, K. S. *Acc. Chem. Res.* **1979**, *12*, 271. (b) Pyykkö, P.; Desclaux, J.-P. *Acc. Chem. Res.* **1979**, *12*, 276.
(21) Norling, B. K.; Steinfink, H. *Inorg. Chem.* **1966**, *5*, 1488.
(22) (a) Lin, W.; Steinfink, H. *Inorg. Chem.* **1965**, *4*, 877. (b) Pardo, M. P.; Flahaut, J. *Bull. Soc. Chim. Fr.* **1967**, 3658.
(23) See, for example: Tremel, W.; Hoffmann, R. *J. Am. Chem. Soc.* **1987**, *109*, 114, and references therein.

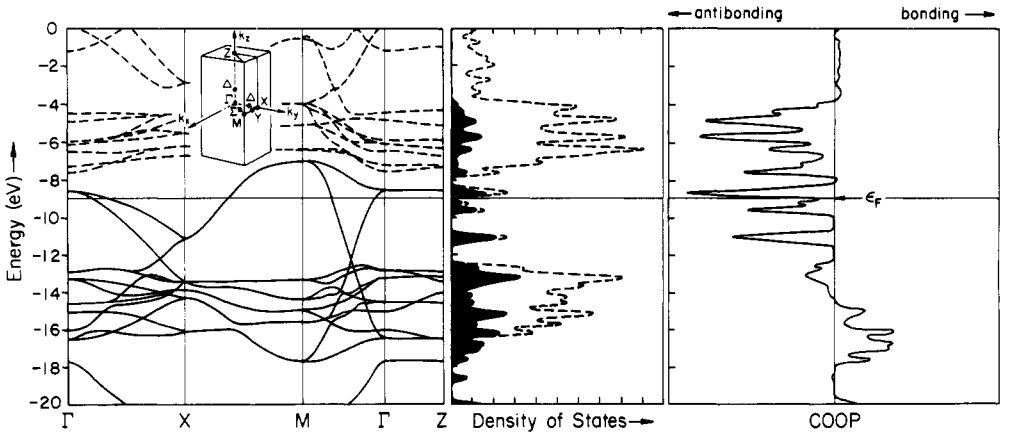

Figure 5. (Left) The band structure of $LaTe_2$. (Middle) Density of states with Te contribution in black. (Right) Te_{II}–Te_{II} crystal orbital overlap population.

shorter than the remaining Te–Te distances and indicate considerable Te–Te bonding and two-dimensional metallic character. The environment of Te_{II} is square pyramidal; the Te_I–Te_{II} distances indicate negligible bonding between the two different types of Te atoms. The Te_I atoms in the $LnTe_2$ structure have four in-plane Te and four additional Ln neighbors; in the $LnTe_3$ structure two cation neighbors of the boundary Te atoms are replaced by four Te neighbors of the adjacent layer sheets. While the $LnTe_2$ compounds are metallic, the physical properties of the $LnTe_3$ phases are varied: $LaTe_3$ is metallic,[24] other such as $PrTe_3$ are semiconducting.[25]

The electronegativity differences in the $LnTe_3$ phases are larger than those in $NbNiTe_5$, and we have no trouble assigning formal oxidation numbers. Therefore a reasonable bonding picture can be obtained from simple electron counting. In the rare-earth-metal compound the cation is certainly trivalent. Counting the Te_{II} atoms as Te^{2-}, the Te_I atoms remain with a total of seven electrons, which renders the p band five-sixths filled. Therefore metallic properties and a small amount of Te–Te bonding can be expected in the $LnTe_2$ compounds. The situation in the $LnTe_3$ compounds is only slightly more complicated. If we count Ln as Ln^{3+} and Te_I as Te^{2-}, then one electron has to be shared between two basal Te atoms. This should yield enhanced bonding between the Te atoms and—in contradiction to the experiment[25]—metallic properties.

Let us start with the Fe_2As-like $LnTe_2$ structure type. Our calculations have been done on $LaTe_2$ as a representative structure with parameters given in the Appendix. As we mentioned in the last section, the structure consists of interpenetrating arrangements of square nets of different mesh. The Ln-based bands are likely to be high in energy. Therefore we are left with the bands of two square nets of different mesh, built by the Te atoms. Following the literature procedure[23,26] we can construct the band structure of a square net in a straightforward manner. The bands of the less dense net are narrow, whereas those of the dense net have a substantial dispersion. The calculated band structure of $LaTe_2$ along four selected symmetry lines is presented in Figure 5. Bands centered on Te_I are drawn as bold lines, and bands centered on La are shown as dashed lines. The similarity of the fragment bands with the energy bands of an individual square net justifies our approach to the structure as a layering of square nets. In addition the flat bands along the line Γ–Z give evidence that the structure is really layerlike. The Fermi level crosses several bands in the $LaTe_2$ structure, and as a consequence the $LnTe_2$ compounds should be good two-dimensional conductors.

Let us focus now on our main point of interest, the Te–Te interactions in the $LaTe_2$ structures. The Te–Te interactions can be traced by means of the COOP curve at the right-hand side of Figure 5. Note the wide, dispersive 5s,p band. Its bottom is Te–Te bonding, the top strongly antibonding. For a $LaTe_2$ electron count, these bands are about to be filled, i.e., we enter the antibonding regime. The numerical value of 0.057 for the Te–Te overlap populations is comparable to the values obtained for the Te_I–Te_I and Te_{II}–Te_{II} overlap populations in $NbNiTe_5$.

For the $LnTe_3$ phases the situation is similar. The DOS decomposition (not given here) shows that the states at the Fermi level are almost exclusively centered on the Te_I and Te_{III} atoms which build up the top and bottom of each layer (see **12**). The structure of the $LnTe_3$ phases differs from that of the $LnTe_2$ compounds by one additional Te atom net which gives these compounds a typical layer character. In the band structures of the $LnTe_3$ compounds we observe the features of an additional square net of Te atoms superimposed on the energy bands of the $LnTe_2$ compounds. The bands are doubled, and they run virtually parallel throughout the whole Brillouin zone. As before, the states centered on the dense square nets are strongly Te–Te antibonding around the Fermi level, but the corresponding bands have to accommodate less electrons compared to $LnTe_2$. As a result the computed Te–Te overlap population of 0.101 is significantly higher than in $LnTe_2$. The Fermi level for $LnTe_3$ rests close to a slight "dip" in the density of states. Nevertheless it cuts several bands along the Γ–X and M–Γ directions of the Brillouin zone. Could any distortion render the material metallic? Any distortion that leads to a loss of the C_2 symmetry along the lines Γ–X and M–Γ must—by symmetry—remove the two band crossings in Figure 5. But for the given band filling the result would not be a semiconductor; according to our calculations the $LnTe_3$ materials should be—in contrast to some of the experimental results[25]—two-dimensional metals.[21]

Pd and Ta Derivatives

Relevant to our intriguing $NbNiTe_5$ structure, two other stoichiometric compounds, namely, $TaNiTe_5$[27] and Nb-

(24) Ramsey, T. H.; Steinfink, H.; Weiss, E. J. *J. Appl. Phys.* **1965**, *36*, 548.
(25) Bucher, E.; Andres, K.; DiSalvo, F. J.; Maita, J. P.; Gossard, A. C.; Cooper, A. S.; Hull, G. W., Jr. *Phys. Rev.* **1975**, *B11*, 500.
(26) Zheng, C.; Hoffmann, R. *Z. Naturforsch.* **1986**, *41B*, 292.
(27) Liimatta, E. W.; Ibers, J. A. *J. Solid State Chem.* **1989**, *78*, 7.

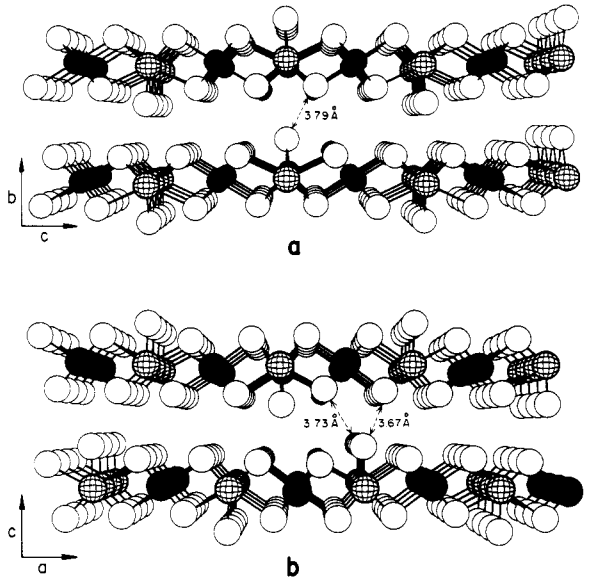

Figure 6. Comparison of the stacking in $NbNiTe_5$ (a) and $NbPdTe_5$ (b).

$PdTe_5$,[28] have been characterized so far.[27] The conductivity of $TaNiTe_5$, isostructural with $NbNiTe_5$, is somewhat greater ($\sigma_{297} = 2.6 \times 10^4$ vs $1.3 \times 10^4\ \Omega^{-1}\ cm^{-1}$). On the other hand the magnetic moment μ_{eff} is slightly weaker (1.03 vs 1.24 μ_B). The metallic conductivity increases while the magnetic susceptibility decreases.

The layers are almost identical in $NbNiTe_5$ and $NbPdTe_5$, but they stack differently as shown Figure 6. Though these compounds are very similar, there is a large difference in their conductivity: $NbNiTe_5$ is highly metallic (vide supra), while $NbPdTe_5$ is less conductive ($\sigma_{295} = 1.3 \times 10^3\ \Omega^{-1}\ cm^{-1}$).[28] Is this difference due to the different stacking of the layers or to the difference in the chemical composition of the layer itself? The shortest contacts between the layers are between tellurium atoms and are 3.79 and 3.67 Å, respectively, for $NbNiTe_5$ and $NbPdTe_5$. Note that the shortest layer–layer separation is associated with the poorest conductor. Weak interaction is expected at such distances. However, in both cases the interlayer separations are shorter than the radius of Te^{2-} (4.4 Å).[29] So, to look at the effect of the different stacking on the electronic properties of these layered compounds, we performed calculations on 3-D $NbNiTe_5$ in two different geometries: one as observed ($NbNiTe_5$) and the other one simulating that of $NbPdTe_5$.[30] The geometry of the $NbPdTe_5$-like structure was constructed by taking $NbNiTe_5$ and translating one layer over two by $0.076b + 0.173c$ to have some interlayer Te···Te contacts of 3.67 Å. The overall electronic structures of the two compounds are almost identical. Fermi levels, atomic charges, and total electron energies per unit cell are comparable. In both cases a slight attractive interaction occurs between the layers through the long Te···Te contacts. The calculated Te···Te overlap populations are rather small but positive 0.004 (3.79 Å) in $NbNiTe_5$ and 0.005 (3.67 Å) and 0.006 (3.73 Å) in $NbPdTe_5$. We particularly compared the band structures of the two geometries along the stacking axis. Flat bands are observed around the Fermi level in both geometries (see Figure 7a for $NbNiTe_5$ and Figure 7b for $NbPdTe_5$). Note that the Fermi level crosses bands only in $NbNiTe_5$. These flat bands possess very little contribution of Te 5p orbitals oriented along the stacking axis, the b axis, and probably do not intervene in the conductivity within the layers. Some bands located somewhat above and below the Fermi level have some contribution of Te 5p orbitals oriented along the stacking axis and therefore are more dispersive as shown in Figure 7. These bands are empty or filled, so the conductivity difference seems to depend on the substitution of Pd for Ni in the layers rather than the different stacking. Conductivity in these ternary chalcogenides results from a compromise between metal–tellurium and tellurium–tellurium interactions. These interactions are perturbed when metal atoms are substituted by others, leading to a change in conductivity behavior. It is beyond the ability of the extended Hückel method to interpret the difference in the metallic behavior of these isoelectronic compounds.

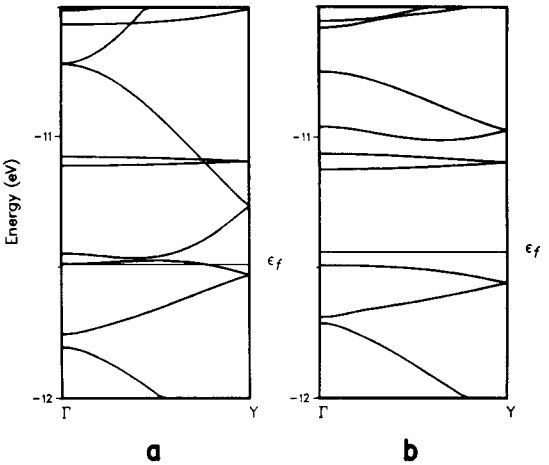

Figure 7. Band structures of $NbNiTe_5$ (a) and $NbPdTe_5$ (b) along the b^* axis.

Table I. Extended Hückel Parameters

orbital	H_{ii}, eV	ζ_1[a]	ζ_2[a]
Nb 5s	−10.10	1.90	
5p	−6.86	1.85	
4d	−12.10	4.08 (0.6401)	1.64 (0.5516)
Ni 4s	−9.70	2.10	
4p	−5.15	2.10	
3d	−13.49	5.75 (0.5798)	2.30 (0.5782)
Te 5s	−20.80	2.51	
5p	−14.00	2.16	
La 5d	−8.21	3.78 (0.7765)	1.38 (0.4586)
6s	−7.67	2.14	
6p	−5.01	2.08	

[a] Exponents and coefficients (in parentheses) in a double-ζ expansion of the metal d orbitals.

Magnetic and metallic properties might be related. Unfortunately magnetic measurements on the Pd derivative have not yet been reported. Further experiments and measurements are expected for this interesting family of compounds.

Conclusions

We have attempted to analyze the electronic structure and bonding in the metallic and paramagnetic $NbNiTe_5$ compound and in some rare-earth-metal polytellurides. Metallic behavior arises primarily from Te 5p carriers. High anisotropic conductivity along the a axis of $NbNiTe_5$ is expected in agreement with experiment. The oxidation formalism $(Nb^{3+})(Ni^{2+})(Te)_5^{5-}$ seems more appropriate than $(Nb^{5+})(Ni^{4+})(Te)_5^{9-}$ in accounting for the numerous Te–Te contacts. This is in agreement with our calculations and the electronegativity scale of the constituent elements. However, there are inherent ambiguities in any oxidation

(28) Liimatta, E. W.; Ibers, J. A. *J. Solid State Chem.* **1988**, *77*, 141.
(29) Shannon, R. D. *Acta Crystallogr.* **1976**, *A32*, 751.
(30) Ni parameters were used for both geometries in the calculations.

state formalism, and these we have discussed. The bonding between tellurium and transition-metal atoms is highly covalent. Weak paramagnetism might result from both itinerant and localized electrons.

Acknowledgment. We thank Prof. F. J. DiSalvo and Dr. E. Canadell for helpful comments. Calculations similar to ours were carried out at the Laboratoire de Chimie Theorique, Université de Paris Sud, by E. Canadell and I. El Idrissi. J.-F.H. thanks Dr. R. L. Johnston for sharing his expertise. His stay at Cornell was made possible by a grant from an exchange program between the NSF and the CNRS. W.T. was supported by a Liebig fellowship from the Verband der Chemischen Industrie. The computing equipment at Münster was purchased through a grant by the Deutsche Forschungsgemeinschaft (DFG, Kr 406/9-1). The work at Cornell was supported by NSF Grant DMR85-16616-AO2. The work at Northwestern University was supported by NSF Solid State Chemistry Grants DMR 83-15554 and DMR 88-13623.

Appendix

The parameters used in the calculations are listed in Table I. The tellurium parameters have been chosen to reproduce self-consistent LMTO-ASA calculations in $NiTe_2$.[9] The experimental geometries of $NbNiTe_5$, $NdTe_2$, and $NdTe_3$ were used for all calculations.

A 21K-point set was used in the rectangle irreducible Brillouin zone for the DOS calculations. The plot of the band structure along high-symetry lines has been made using the space group D_{2h}^5-*Pmcm* (*Pmma*, no. 51) to account for the thickness of the two-dimensional $NbNiTe_5$ slab. For $LaTe_2$ and $LaTe_3$ a 27K-point set was used in the irreducible wedge of the Brillouin zone.

Registry No. $NiNbTe_5$, 113671-41-3.

A Designed Fluid Cracking Catalyst with Vanadium Tolerance

C. A. Altomare,*[1] G. S. Koermer,[1] P. F. Schubert,[2] S. L. Suib,[3] and W. S. Willis[3]

Engelhard Corporation, Menlo Park, CN 40, Edison, New Jersey 08818, and Department of Chemistry and Institute of Materials Science, University of Connecticut, Storrs, Connecticut 06268

Received February 6, 1988

A fluid cracking catalyst with two functions, strong acid zeolitic cracking and vanadium passivation, was designed. Vanadium passivation is important for maintaining cracking catalyst performance when processing heavy petroleum feedstocks. The catalyst was made by growing zeolite Y on the external and internal surface of microspheres containing the vanadium trap forsterite. Surface spectroscopy and catalytic results were used to demonstrate that the catalyst was synthesized as designed and that both the cracking function and vanadium trapping function were preserved.

Introduction

Molecular design of materials is a subject of recent interest. The objective of molecular design is to control the physical and chemical properties of a material by carefully controlling the structure and composition of the material. Modification of electrode surfaces to enhance electrocatalytic activity,[4] encapsulation of organometallics in zeolites[5] and layered solids,[6] and control of the size, shape, and composition of optical and electronic materials such as ceramics[7] and second harmonic generators[8] are current areas of interest that involve molecular design of materials.

In this work, molecular design has been applied to cracking catalyst synthesis. Modern cracking catalysts are approximately 70-μm-diameter microspheres containing zeolite Y in a matrix material such as silica alumina. One of the many challenges in catalytic cracking of hydrocarbons is to create materials including both active cracking functions (e.g., zeolite Y) and contaminant scavengers or passivators. Cracking catalyst activity and selectivity are greatly reduced by crude oil contaminants such as nickel, vanadium, and other metals.[9-13] Certain additives incorporated into the catalyst matrix could reduce contaminant effects. Alkaline-earth metal oxides can immobilize vanadium, preventing it from destroying the zeolite, and may also reduce vanadium's undesirable coke and hydrogen making tendencies.[9,10,14-18]

Modern cracking catalyst preparation follows two main routes. The most common involves spray drying cation-

(1) Engelhard Corporation.
(2) Present address: Phillips Petroleum, Bartlesville, OK 74004.
(3) University of Connecticut.
(4) Miller, J. S., Ed. *Chemically Modified Surfaces in Catalysis and Electrocatalysis*; ACS Symposium Series 192; American Chemical Society: Washington, DC, 1982. Zak, J.; Kuwana, T. *J. Electroanal. Chem. Interfacial Electrochem.* **1983**, *150*, 645-664.
(5) Zerger, R. P.; McMahon, K. C.; Seltzer, M. D.; Michel, R. G.; Suib, S. L. *J. Catal.* **1986**, *99*, 498-505.
(6) Pinnavia, T. J. *Science* **1983**, *220*, 365-471.
(7) Lackey, W. J.; Stinton, D. P.; Cerny, G. A.; Scaffhauser, A. C.; Fehrenbacher, L. L. *Adv. Ceram. Mater.* **1987**, *2*, 24-30.
(8) Eddy, M. M.; Gier, T. E.; Keder, N. L.; Stucky, G. D.; Cox, D. E.; Bierlein, J. D.; Jones, G. *Inorg. Chem.* **1988**, *27*, 1856-1858.
(9) Schubert, P. F. *Prepr.—Am. Chem. Soc., Div. Pet. Chem.* **1987**, *32*, 673-676.
(10) Schubert, P. F.; Altomare, C. A. *ACS Symp. Ser.* **1988**, *375*, 182-194.
(11) Occelli, M. L.; Kowalczyk, D. C.; Kibby, C. L. *Appl. Catal.* **1985**, *16*, 227-236.
(12) Grane, H. R.; Conner, J. E.; Masologites, G. P. *Proc., Am. Pet. Inst., Sect. 3* **1961**, *41*, 241-246.
(13) Rothrock, J. J.; Birkhimer, E. R.; Leum, L. N. *Ind. Eng. Chem.* **1957**, *49*, 272-276.
(14) Wormsbecher, R. F.; Peters, A. W.; Maselli, J. M. *J. Catal.* **1986**, *100*, 130-137.
(15) Occelli, M. L. *Prepr.—Am. Chem. Soc., Div. Pet. Chem.* **1987**, *32*, 658-662.
(16) Bell, V. A.; Schubert, P. F.; Turner, G.; Jacobs, V. Federation of Analytical Chemistry and Spectroscopy Societies, Meeting XIV, Detroit, Oct 1987.
(17) Mitchell, B. R.; Vogel, R. F. U.S. Patent 4,451,355, 1984.
(18) Kugler, E. L.; Rhodes, R. P. U.S. Patent 4,743,358, 1988.

0897-4756/89/2801-0459$01.50/0